Generation of three wide frequency bands within a single white-light cavity

Anas Othman,[1,2,*] David Yevick,[1,†] and M. Al-Amri[3,4,‡]

[1]*Department of Physics, University of Waterloo, 200 University Avenue West, Waterloo, ON, Canada N2L 3G1*

[2]*Department of Physics, Faculty of Science, Taibah University, P.O. Box 344, Al Madinah Al Munawwarah, Saudi Arabia*

[3]*The National Center for Applied Physics, KACST, P.O. Box 6086, Riyadh 11442, Saudi Arabia*

[4]*Department of Physics, KKU, P.O. Box 9004, Abha 61413, Saudi Arabia*

(Received 14 September 2017; published 9 April 2018)

We theoretically investigate the double-Λ scheme inside a Fabry-Pérot cavity employing a weak probe beam and two strong driving fields together with an incoherent pumping mechanism. By generating analytical expressions for the susceptibility and applying the white-light cavity conditions, we devise a procedure that reaches the white-light condition at a smaller gas density than the values typically cited in similar previous studies. Further, when the intensities of the two driving fields are equal, a single giant white band is obtained, while for unequal driving fields three white bands can be present in the cavity. Two additional techniques are then advanced for generating three white bands and a method is described for displacing the center frequency of the bands. Finally, some potential applications are suggested.

DOI: 10.1103/PhysRevA.97.043816

I. INTRODUCTION

Optical switches have found numerous applications, including gravitational waves in signal recycling mirrors (SRMs) [1,2], Q-switched lasers [3,4], and control of entanglement in trapped qubits [5], and in quantum circuits and quantum networks [6–8]. Previously suggested optical switching mechanisms based on controlling the transmission of light in a cavity through the interaction of an atomic system with the electromagnetic field include applying a driving field to an two-level atomic gas [9], a Λ three-level atomic gas in the presence of two coupling fields [10,11], and a low light output confocal cavity containing a double-Λ four-level atom system utilizing a rubidium atomic vapor cell [12]. Alternative suggestions employ a microtoroidal resonator coupled to an optical fiber [13] and electromagnetically induced gratings (EIGs) [14–16]. However, most of these methods suffer from mechanical instability and generally only operate within a single narrow frequency band.

Accordingly, in a recent article, one of us (M.A.), together with co-workers [17], instead investigated white-light cavities (WLCs) based on Λ atomic gas. Unlike standard cavities that resonate at discrete frequencies determined by the optical round-trip length, WLCs resonate over a broad and continuous range of frequencies [18–22] and have consequently already been employed in data buffering [23–25] and measurement [26–28] applications.

In the design of Ref. [17], a system of Λ gas atoms in an optically pumped Fabry-Pérot cavity with a broad white-light band was employed. By changing the intensity of the driving fields and the atomic density, the frequency width of this band and the associated cavity reflection can be reduced to zero. As a result, such a system can be potentially employed as an optical switch. However, similar to the previous cited methods, this procedure is limited to a single band with a center frequency that is typically determined by system parameters such as the atomic spacing and decay rates that cannot be easily be controlled. In this article, we accordingly propose three different procedures based on a four-level double-Λ atomic gas within an optically pumped Fabry-Pérot cavity. By appropriately tuning the driving fields, we realize three independent procedures for generating up to three broad frequency bands with tunable center frequencies in place of a single band.

The article is organized as follows. First, in Sec. II, the double-Λ model is described. Sections III and IV then present the analytical formulation and derive appropriate formulas for the electromagnetic susceptibility. In Sec. V, the white-light cavity conditions are presented. Subsequently, the method employed to generate a single white-light band follows in Sec. VI while the three procedures (A, B, and C) for generating three white bands follow in Secs. VII A and VII B. Section VIII then describes a strategy for displacing the center of broad white bands. In Sec. IX, we demonstrate some potential applications for our results. Section X finally contains the conclusions of the paper.

II. MODEL DESCRIPTION

Optical control of parameters such as the susceptibility and the refractive index in an atomic gas can be employed to exploit effects such as electromagnetically induced transparency (EIT) [29,30], a negative refractive index [31,32], and reflective index enhancement without absorption [33]. In this article, the susceptibility of an atomic gas confined inside a Fabry-Pérot cavity is engineered to produce several transmission bands that can be controlled by modulating the intensity of external

*a2othman@uwaterloo.ca
†yevick@uwaterloo.ca
‡mdalamri@kacst.edu.sa

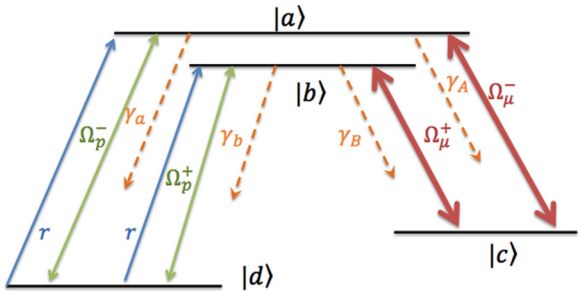

FIG. 1. The level structures, decay rates, and external fields of the double-Λ scheme.

fields. That is, several fields are employed inside the cavity to modify the susceptibility of the atomic gas which interacts with electromagnetic radiation according to the four-level double-Λ scheme of Fig. 1.

The scheme has four levels $|a\rangle$, $|b\rangle$, $|c\rangle$, and $|d\rangle$, where $|a\rangle$ denotes the upper level. Two weak probe fields couple three levels: levels $|a\rangle$ and $|d\rangle$ characterized by the Rabi frequency Ω_p^-, and levels $|b\rangle$–$|d\rangle$ with Rabi frequency Ω_p^+. One strong driving field additionally couples $|a\rangle$ and $|c\rangle$ with Rabi frequency Ω_μ^- while a second applies $|b\rangle$ and $|c\rangle$ with Rabi frequency Ω_μ^+. Two incoherent pumping mechanisms additionally couple levels $|a\rangle$ and $|d\rangle$ and $|b\rangle$ and $|d\rangle$ with a pumping rate denoted by r. The decay rates from the exited states equal γ_a from $|a\rangle$ to $|d\rangle$, γ_b from $|b\rangle$ to $|d\rangle$, γ_A from $|a\rangle$ to $|c\rangle$, and, finally, γ_B from $|b\rangle$ to $|c\rangle$. The decay rates from $|c\rangle$ and $|d\rangle$ are assumed to be zero.

Various experimental implementations of the above double-Λ scheme exist [34–36]. For example, in the rubidium [37] or sodium [38] gas two hyperfine ground levels with $F = 1$ and $F = 2$ are present, and the states $|d\rangle$ and $|c\rangle$ then correspond to the $M_F = -1$ and $M_F = 1$ magnetic sublevels of the $F = 1$ hyperfine ground level, while the upper states $|a\rangle$ and $|b\rangle$ in our notation are the $M_F = 0, F = 1$ and $M_F = 0, F = 2$ excited states. In this case, two oppositely circularly polarized counterpropagating fields $\sigma^\pm$ must be employed for the drive and probe fields.

III. ANALYTIC FORMULATION

After applying the dipole approximation and the rotating wave approximation (RWA) the Hamiltonian of the double-Λ scheme becomes

$$\hat{H} = \hbar\Big[\sum_i^{a,b,c,d} \omega_i |i\rangle\langle i| - \frac{\Omega_p^-}{2} e^{i\Delta_1 t}|a\rangle\langle d| - \frac{\Omega_p^+}{2} e^{i\Delta_2 t}|b\rangle\langle d| - \frac{\Omega_\mu^+}{2} e^{i\Delta_3 t}|b\rangle\langle c| - \frac{\Omega_\mu^-}{2} e^{i\Delta_4 t}|a\rangle\langle c| + \text{H.c.}\Big], \quad (1)$$

in which $\hbar\omega_i$ is the energy of the level $|i\rangle$ and the Rabi frequencies of the probe fields are $\Omega_p^- = |d_{ad}|E/\hbar$ and $\Omega_p^+ = |d_{bd}|E/\hbar$, in which E is the electric field of the probe field and the driving field Rabi frequencies are $\Omega_\mu^+ = |d_{bc}|E_\mu^+/\hbar$, $\Omega_\mu^- = |d_{ac}|E_\mu^-/\hbar$. The detuning parameters Δ_i are given by $\Delta_1 = \omega_{ad} - \omega_p^-$, $\Delta_2 = \omega_{bd} - \omega_p^+$, $\Delta_3 = \omega_{bc} - \omega_\mu^+$, and $\Delta_4 = \omega_{ac} - \omega_\mu^-$. Here, $\omega_{ij} = \omega_j - \omega_i$ while $\omega_p^\pm$ and $\omega_\mu^\pm$ denote the frequencies of the probe and driving fields, respectively.

A stable steady state only exists in the double-Λ scheme if the frequencies of the interacting beams satisfy the condition

$$\omega_p^- - \omega_p^+ = \omega_\mu^- - \omega_\mu^+ \quad (2)$$

[39,40], as is easily verified by applying the Hamiltonian of Eq. (1) to the master equation below. In the following analysis, the frequencies of the probe and driving beams are set to $\omega_p^- = \omega_p^+ = \omega$, and $\omega_\mu^+ = \omega_\mu^- = \omega_\mu$. Accordingly, only one probe field with frequency ω is present while the frequency of both driving fields equals ω_μ. The detuning parameters Δ_i are then $\Delta_1 = \omega_{ad} - \omega$, $\Delta_2 = \omega_{bd} - \omega$, $\Delta_3 = \omega_{bc} - \omega_\mu$, and $\Delta_4 = \omega_{ac} - \omega_\mu$. The master equation then takes the form

$$\dot{\hat{\rho}} = -\frac{i}{\hbar}[\hat{H}, \hat{\rho}], \quad (3)$$

in terms of the density-matrix operator $\hat{\rho}$. After applying the Hamiltonian of Eq. (1) to the master equation, inserting the expressions for the decay rates and the pumping rates, and transforming in standard fashion, one obtains

$$\dot{\rho}_{aa} = -(\gamma_a + \gamma_A)\rho_{aa} + r\rho_{dd} + \frac{i}{2}(\tilde{\rho}_{ac}\Omega_\mu^{-*} - \tilde{\rho}_{ad}\Omega_p^{-*} + \text{H.c.}), \quad (4)$$

$$\dot{\rho}_{bb} = -(\gamma_b + \gamma_B)\rho_{bb} + r\rho_{dd} + \frac{i}{2}(\tilde{\rho}_{bd}\Omega_p^{+*} - \tilde{\rho}_{bc}\Omega_\mu^{+*} + \text{H.c.}), \quad (5)$$

$$\dot{\rho}_{cc} = \gamma_A\rho_{aa} + \gamma_B\rho_{bb} + \frac{i}{2}(\tilde{\rho}_{bc}\Omega_\mu^{+*} + \tilde{\rho}_{ac}\Omega_\mu^{-*} + \text{H.c.}), \quad (6)$$

$$\dot{\rho}_{dd} = -2r\rho_{dd} + \gamma_a\rho_{aa} + \gamma_b\rho_{bb} + \frac{i}{2}(\tilde{\rho}_{ad}\Omega_p^{-*} + \tilde{\rho}_{bd}\Omega_p^{+*} + \text{H.c.}), \quad (7)$$

$$\dot{\tilde{\rho}}_{ab} = -\gamma_{ab}\tilde{\rho}_{ab} - 2i\omega_{ab}\tilde{\rho}_{ab} + \frac{i}{2}(\tilde{\rho}_{cb}\Omega_\mu^- + \tilde{\rho}_{db}\Omega_p^- - \tilde{\rho}_{ad}\Omega_p^{+*} - \tilde{\rho}_{ac}\Omega_\mu^{+*}), \quad (8)$$

$$\dot{\tilde{\rho}}_{ac} = -\gamma_{ac}\tilde{\rho}_{ac} - i(\Delta_\mu + \omega_{ab})\tilde{\rho}_{ac} + \frac{i}{2}[-\tilde{\rho}_{ab}\Omega_\mu^+ + (\rho_{cc} - \rho_{aa})\Omega_\mu^- + \tilde{\rho}_{dc}\Omega_p^-], \quad (9)$$

$$\dot{\tilde{\rho}}_{ad} = -\gamma_{ad}\tilde{\rho}_{ad} + i(\Delta - \omega_{ab})\tilde{\rho}_{ad} + \frac{i}{2}[-\tilde{\rho}_{ab}\Omega_p^+ + \tilde{\rho}_{cd}\Omega_\mu^- - (\rho_{aa} - \rho_{dd})\Omega_p^-], \quad (10)$$

$$\dot{\tilde{\rho}}_{bc} = -\gamma_{bc}\tilde{\rho}_{bc} - i(\Delta_\mu - \omega_{ab})\tilde{\rho}_{bc} + \frac{i}{2}[\tilde{\rho}_{dc}\Omega_p^- - (\rho_{bb} - \rho_{cc})\Omega_\mu^+ - \tilde{\rho}_{ba}\Omega_\mu^-], \quad (11)$$

$$\dot{\tilde{\rho}}_{bd} = -\gamma_{bd}\tilde{\rho}_{bd} + i(\Delta + \omega_{ab}) + \frac{i}{2}[\tilde{\rho}_{cd}\Omega_\mu^+ - \tilde{\rho}_{ba}\Omega_p^- - (\rho_{bb} - \rho_{dd})\Omega_p^+], \quad (12)$$

$$\dot{\tilde{\rho}}_{cd} = -\gamma_{cd}\tilde{\rho}_{cd} + i(\Delta_\mu + \Delta)\tilde{\rho}_{cd} + \frac{i}{2}(-\tilde{\rho}_{cb}\Omega_p^+ - \tilde{\rho}_{ca}\Omega_p^- + \tilde{\rho}_{bd}\Omega_\mu^{+*} + \tilde{\rho}_{ad}\Omega_\mu^{-*}), \quad (13)$$

where $\tilde{\rho}_{ij}$ is the density-matrix element after the transformations and $\gamma_{ij} \equiv (\gamma_i + \gamma_j)/2$. The detuning parameters

appearing in the above equation are defined by $\Delta = \omega - W = \omega - \omega_{ad} - \omega_{bd}$ and $\Delta_\mu = Q - \omega_\mu = \omega_{ac} + \omega_{bc} - \omega_\mu$, where W is $\omega_{ad} + \omega_{bd}$ and $Q = \omega_{ac} + \omega_{bc}$. In this manner, the values of the energies ω_{ad}, ω_{bc}, ω_{bc}, and ω_{bd} do not need to be determined individually as only ω_{ab} appears.

To find the steady-state matrix elements, $\dot{\tilde{\rho}}_{ij} = 0$, and the two associated elements of the probe field, $\tilde{\rho}_{ad}$ and $\tilde{\rho}_{bd}$, the above equations are solved algebraically. Since the probe field is weak, $\Omega_p^\pm$ is only retained to first order, while the strong driving fields $\Omega_\mu^\pm$ are kept to the second order. Solving Eqs. (5)–(10) then yields

$$\tilde{\rho}_{bd}^{(1)} = \frac{i}{D_{bd} + \frac{|\Omega_\mu^+|^2}{4D_{cd}}}\left[\Omega_p^+\left(\frac{|\Omega_\mu^+|^2}{8D_{cd}D_{bc}^*}P_{bc} - \frac{1}{2}P_{bd}\right) - \Omega_p^-\left(\frac{\Omega_\mu^+\Omega_\mu^{-*}}{8D_{cd}D_{ac}^*}P_{ca}\right)\right], \tag{14}$$

$$\tilde{\rho}_{ad}^{(1)} = \frac{i}{D_{ad} + \frac{|\Omega_\mu^-|^2}{4D_{cd}}}\left[\Omega_p^+\left(\frac{\Omega_\mu^-\Omega_\mu^{+*}}{8D_{cd}D_{bc}^*}P_{bc}\right) - \Omega_p^-\left(\frac{|\Omega_\mu^-|^2}{8D_{cd}D_{ac}^*}P_{ca} + \frac{1}{2}P_{ad}\right)\right], \tag{15}$$

where $P_{ij} = \rho_{ii} - \rho_{jj}$ and $\tilde{\rho}_{ij}^{(1)}$ denote the population difference and the first-order approximation of the probe field of element $\tilde{\rho}_{ij}$ while the different D_{ij} parameters are defined by $D_{bd} = \gamma_{bd} - i(\Delta + \omega_{ab})$, $D_{ad} = \gamma_{ad} - i(\Delta - \omega_{ab})$, $D_{cd} = \gamma_{cd} - i(\Delta_\mu + \Delta)$, $D_{bc} = \gamma_{bc} + i(\Delta_\mu - \omega_{ab})$, and $D_{ac} = \gamma_{ac} + i(\Delta_\mu + \omega_{ab})$.

The electric susceptibility χ is the sum of the contributions χ_{ad} and χ_{bd} from each of the interactions of the probe field as

$$\begin{aligned}\chi\epsilon_0 E/2 &= |d_{ad}|\tilde{\rho}_{ad}^{(1)} + |d_{bd}|\tilde{\rho}_{bd}^{(1)},\\ \chi &= 2|d_{ad}|\tilde{\rho}_{ad}^{(1)}/(\epsilon_0 E) + 2|d_{bd}|\tilde{\rho}_{bd}^{(1)}/(\epsilon_0 E),\\ \chi &= \chi_{ad} + \chi_{bd},\end{aligned} \tag{16}$$

Substituting Eqs. (14) and (15) into Eq. (16) then yields

$$\chi_{bd} = \frac{i}{D_{bd} + \frac{|\Omega_\mu^+|^2}{4D_{cd}}}\left[\mathcal{C}\left(\frac{|\Omega_\mu^+|^2}{4D_{cd}D_{bc}^*}P_{bc} - P_{bd}\right) - \mathcal{B}\left(\frac{\Omega_\mu^+\Omega_\mu^{-*}}{4D_{cd}D_{ac}^*}P_{ca}\right)\right], \tag{17}$$

$$\chi_{ad} = \frac{i}{D_{ad} + \frac{|\Omega_\mu^-|^2}{4D_{cd}}}\left[\mathcal{B}\left(\frac{\Omega_\mu^-\Omega_\mu^{+*}}{4D_{cd}D_{bc}^*}P_{bc}\right) - \mathcal{A}\left(\frac{|\Omega_\mu^-|^2}{4D_{cd}D_{ac}^*}P_{ca} + P_{ad}\right)\right]. \tag{18}$$

Here, the strength parameters are defined by

$$\mathcal{A} = \frac{N|d_{ad}|^2}{\hbar\epsilon_0}, \quad \mathcal{B} = \frac{N|d_{ad}||d_{bd}|}{\hbar\epsilon_0}, \quad \mathcal{C} = \frac{N|d_{bd}|^2}{\hbar\epsilon_0}. \tag{19}$$

The contribution from all atoms is obtained by multiplying the atomic susceptibility by the number of atoms per unit volume N. The exact expressions for the atomic populations ρ_{ii} are then derived by solving Eqs. (4)–(4) together with the normalization condition $\rho_{aa} + \rho_{bb} + \rho_{cc} + \rho_{dd} = 1$, which gives

$$\rho_{aa}^{(0)} = r\frac{R_a(\gamma_b + \gamma_B) + \gamma_B R_a + \gamma_b R_b + 2R_a R_b}{a_1 R_a + a_2 R_b + a_3 R_a R_b + a_4}, \tag{20}$$

$$\rho_{bb}^{(0)} = r\frac{R_b(\gamma_a + \gamma_A) + \gamma_a R_a + \gamma_A R_b + 2R_a R_b}{a_1 R_a + a_2 R_b + a_3 R_a R_b + a_4}, \tag{21}$$

$$\rho_{dd}^{(0)} = \frac{\gamma_a\rho_{aa}^{(0)} + \gamma_b\rho_{bb}^{(0)}}{2r}, \tag{22}$$

$$\rho_{cc}^{(0)} = 1 - \rho_{aa}^{(0)} - \rho_{bb}^{(0)} - \rho_{cc}^{(0)}, \tag{23}$$

in which $\rho_{ii}^{(0)}$ designates the zero-order probe field, and

$$R_a = \frac{\gamma_{ac}|\Omega_\mu^-|^2}{2\left[\gamma_{ac}^2 + (\Delta_\mu + \omega_{ab})\right]}, \quad R_b = \frac{\gamma_{bc}|\Omega_\mu^+|^2}{2\left[\gamma_{bc}^2 + (\Delta_\mu - \omega_{ab})\right]}, \tag{24}$$

$a_1 = \gamma_a(\gamma_b + \gamma_B) + r(4\gamma_B + 2\gamma_b + \gamma_a)$, $a_2 = \gamma_b(\gamma_a + \gamma_A) + r(4\gamma_A + 2\gamma_a + \gamma_b)$, $a_3 = 6r + \gamma_b + \gamma_a$, and $a_4 = r(2\gamma_A\gamma_B + \gamma_A\gamma_b + \gamma_B\gamma_a)$.

To illustrate the behavior of the susceptibility, the above equations are evaluated with standard parameter values. With $\gamma = 10^7$ the decay parameters employed here are $\gamma_a = \gamma_b = \gamma$, $\gamma_A = \gamma_B = 0.2\gamma$, $\gamma_{ab} = \gamma_{cd} = 0$, and $\gamma_{ac} = \gamma_{bc} = \gamma_{ad} = \gamma_{bd} = (\gamma_a + \gamma_A)/2 = 0.6\gamma$. The density parameters are similarly given in terms of $\mathcal{C}$ by $\mathcal{A} = \theta\mathcal{C}$ and $\mathcal{B} = \Phi\mathcal{C}$, with θ and Φ set to 1.1 and 1.05, respectively. The driving fields are expressed in terms of Ω_μ^- by $\Omega_\mu^+ = \Omega_\mu^-/\alpha$, where α corresponds to the ratio between the two fields. These fields are assumed to be well detuned so that $\Delta_\mu = 0$, while the level spacing $\omega_{ab} = \gamma$. A detuning parameter is additionally defined as $\Delta = \omega - W$, where for typical gases in the optical limit $W = 10^6\gamma$. Accordingly, the following sections examine the dependence of the susceptibility on the free parameters r, Ω_μ^-, α, and $\mathcal{C}$.

IV. SUSCEPTIBILITY

To evaluate the susceptibility, Eq. (16), it is convenient to set $\mathcal{C} = \gamma$ since the susceptibility scales linearly with $\mathcal{C}$. The following cases are then distinguished.

A. $\Omega_\mu^- = \Omega_\mu^+, \alpha = 1$

Since all systems with $r < \gamma$ possess the same inversion properties, they can be analyzed by setting the pumping rate r to zero such that only the state $|d\rangle$ is populated and then increasing the pumping rate up to a value of γ. This insures that the atomic population is primarily in the ground state and therefore $\rho_{aa}^{(0)}, \rho_{bb}^{(0)} - \rho_{dd}^{(0)} < 0$. For the two driving fields with $\alpha = 1$, a pumping rate $r < \gamma$, the susceptibility exhibits EIT as evident from Fig. 2(a) for which the driving field $\Omega_\mu^- = 10\gamma$ and the pumping rate $r = 0.5\gamma$. Evidently, the absorption which is proportional to $\mathrm{Im}(\chi)$ is ≈ 0 over an interval given approximately by $-4\gamma < \Delta < 4\gamma$, while $\mathrm{Re}(\chi)$ displays a linear dispersion with positive slope. In Fig. 2(c), the driving field is set instead to $\Omega_\mu^- = 20\gamma$ with the identical pumping rate as Fig. 2(a), leading to an increase in the width of the near-zero

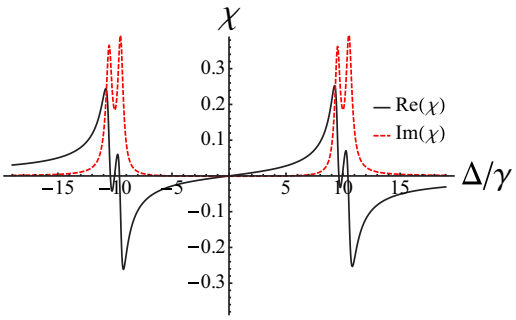

(a) $r = 0.5\gamma$, $\Omega_\mu^- = 20\gamma$

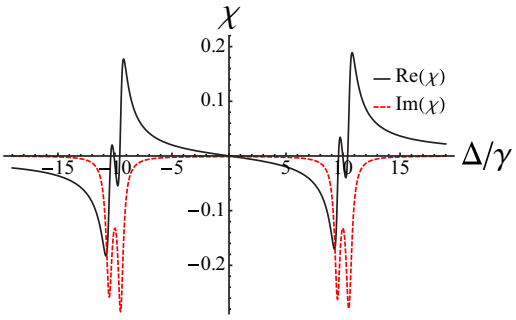

(b) $r = 2\gamma$, $\Omega_\mu^- = 20\gamma$

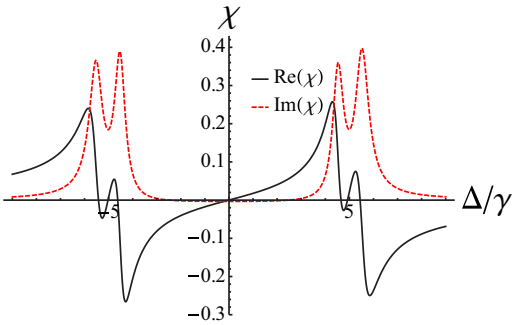

(c) $r = 0.5\gamma$, $\Omega_\mu^- = 10\gamma$

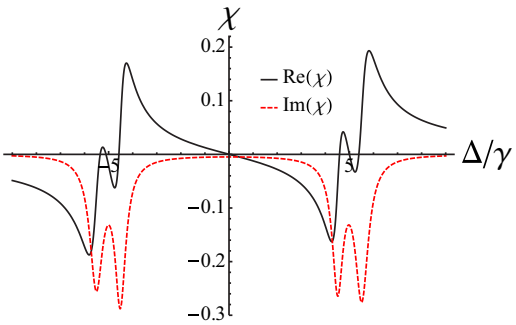

(d) $r = 2\gamma$, $\Omega_\mu^- = 10\gamma$

FIG. 2. The real and imaginary parts of χ for different r and Ω_μ^- with $\alpha = 1$. The real and imaginary parts of χ are show as the solid black and dashed red curves, respectively.

absorption region to $-9\gamma < \Delta < 9\gamma$ but otherwise the same behavior as Fig. 2(a). In fact if the near zero absorption width is denoted by T, then for large driving fields in our system $T \approx \Omega_\mu^-$ over a region from $\Delta \approx -\Omega_\mu^-/2$ and to $\Delta \approx \Omega_\mu^-/2$. That is, the width of the EIT can be manipulated by modulating the amplitude of the driving fields.

For $r > \gamma$, the population inversion becomes positive, with the result that both $\rho_{aa}^{(0)}$ and $\rho_{bb}^{(0)}$ exceed $\rho_{dd}^{(0)}$. In this case, Figs. 2(b) and 2(d) indicate that EIT is again present but that the dispersion slope reverses sign. As in the $r < \gamma$ case, the width of the negative absorption region is given by $T \approx \Omega_\mu^-$. Note that in all of the figures in Fig. 2, two peaks are present on each side of the absorption line. Since these are associated with ω_{ab}, their positions can be altered by changing the value of ω_{ab}. Thus, the width of the EIT and the sign of the dispersion slope can be easily controlled by adjusting the amplitude of the driving fields.

B. $\Omega_\mu^- \neq \Omega_\mu^+, \alpha \neq 1$

Next, the case that α differs from unity (and $\alpha \neq 0,\infty$) so that the intensities of the driving fields differ (note that systems with reciprocal values of α are nearly equivalent) is investigated. In Figs. 3(a) and 3(b), χ is plotted for $\alpha = 2$, $\Omega_\mu^- = 20\gamma$ and $r = 0.5\gamma$ and $r = 2\gamma$, respectively. In both figures three separate regions exist in which $\mathrm{Im}(\chi)$ and hence the absorption is nearly zero. The width of the middle region is $\approx 10\gamma$, while the widths of the left and right regions are $\approx 5\gamma$. However, in Fig. 3(a) with $r = 0.5\gamma$, the three regions exhibit EIT behavior, while in Fig. 3(b) the dispersion slope is negative. In both cases, the width of the middle region is $T \approx \Omega_\mu^-/\alpha$, while that of the two side regions is $T \approx \Omega_\mu^-(\alpha - 1)/(2\alpha)$.

If one of the driving fields is absent, $\alpha \to 0,\infty$, only two zero absorption regions exist, as evident from Figs. 3(c) and 3(d). Similarly, whether the EIT or the negative dispersion behavior is present depends on the value of r. Therefore, changing the ratio of the driving fields strongly influences the widths of the low absorption regions. In the following, we will focus on systems with finite values of α and hence three EIT or negative dispersion regions. The two-region $\alpha \to \infty,0$ case, however, is entirely analogous.

To describe Figs. 3(a) and 3(b) and other cases with $\alpha > 1$ we denote the left, middle, and right negative dispersion regions of Δ with negligible absorption by (-1), (0), and $(+1)$, respectively. The point within each region at which $\mathrm{Re}(\chi) = 0$ is further termed the center point of the region and are labeled as Δ_-, Δ_0, and Δ_+ with $\Delta_- \approx -|\Omega_\mu^-|(\alpha + 1)/(4\alpha)$, 0, and $\Delta_+ \approx +|\Omega_\mu^-|(\alpha + 1)/(4\alpha)$, respectively. In summary, by manipulating the relative amplitude of the driving fields, one, two, or three regions exhibiting EIT or negative dispersion can be obtained. These regions will be employed to generate three white bands in the following sections.

V. WHITE CAVITY CONDITIONS

While a Fabry-Pérot cavity supports discrete resonant frequencies at

$$k_m l = \mathrm{Re}[n(\omega)] l \omega_m / c = m\pi, \quad m = 1,2,3,\ldots, \tag{25}$$

where $n(\omega)$, l, and ω_m are the cavity refractive index, length, and resonant frequencies, for a white-light cavity (WLC) such as that generated by bifrequency Raman gain [18,20,22], a continuous band of frequencies is resonant simultaneously inside the cavity. In a WLC the cavity condition Eq. (25) must

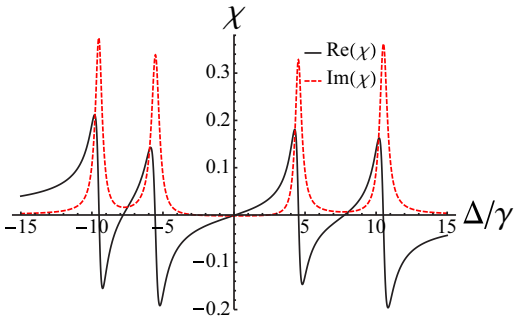

(a) $r = 0.5\gamma$, $\Omega_\mu^- = 20\gamma$, $\alpha = 2$

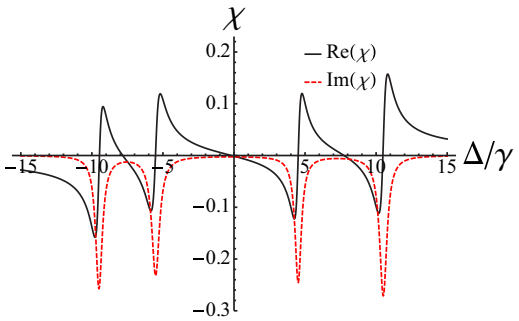

(b) $r = 2\gamma$, $\Omega_\mu^- = 20\gamma$, $\alpha = 2$

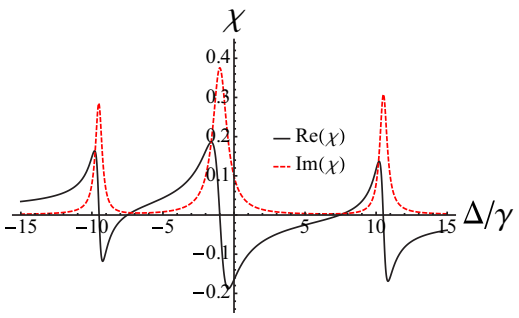

(c) $r = 0.5\gamma$, $\Omega_\mu^- = 20\gamma$, $\alpha \to \infty$

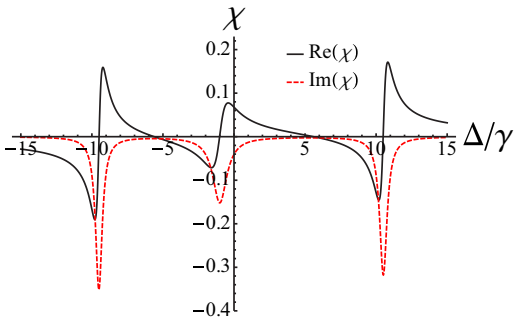

(d) $r = 2\gamma$, $\Omega_\mu^- = 20\gamma$, $\alpha \to \infty$

FIG. 3. The real (solid black) and imaginary (dashed red) parts of χ for different values of r and Ω_μ^- for $\alpha > 1$.

be satisfied for the center points together with a negative and roughly linear dispersion and phase delay cancellation. As seen already in Figs. 2(b), 2(d), 3(b), and 3(d), the negative dispersion condition is realized within adjustable wavelength bands if the pumping $r > \gamma$.

The phase delay condition is derived from Eq. (25) which, however, yields discrete frequencies rather than the continuous band of a WLC. Accordingly, Eq. (25) must first be differentiated with respect to ω where

$$\frac{d\{\omega\,\mathrm{Re}[n(\omega)]\}}{d\omega} = \omega\frac{d\{\mathrm{Re}[n(\omega)]\}}{d\omega} + \mathrm{Re}[n(\omega)] = 0. \quad (26)$$

In the presence of negative dispersion $\mathrm{Re}[n(\omega)]$ can equal the negative of the first term. For the cases when the two driving fields possess equal amplitudes, $\alpha = 1$, the center point of the negative dispersion is $\Delta = 0$ corresponding to $\omega = W$. Since $\chi(W) \approx 0$ near this point, the refractive index $n(\omega) \approx 1$ and Eq. (26) implies

$$\left.\frac{d\{\mathrm{Re}[n(\omega)]\}}{d\omega}\right|_{\omega=W} = -\frac{1}{W}. \quad (27)$$

The slope near the center point is roughly linear, hence the derivative can be approximated as

$$\left.\frac{d\{\mathrm{Re}[n(\omega)]\}}{d\omega}\right|_{\omega=W} \approx \frac{\mathrm{Re}[n(W+\gamma)] - \mathrm{Re}[n(W-\gamma)]}{2\gamma}. \quad (28)$$

Next, the refractive index can be expanded as $n(\omega) = \sqrt{1+\chi(\omega)} \approx 1 + \chi'(\omega)/2 + i\chi''(\omega)/2$, in which $\chi'(\omega)$ and $\chi''(\omega)$ are the real and imaginary parts of the susceptibility, respectively. The final form of the white-light condition for equal driving fields is then

$$\chi'(W+\gamma) - \chi'(W-\gamma) = -\frac{4\gamma}{W}. \quad (29)$$

This equation can be employed to determine the required value of Ω_μ^- for the driving field that satisfies the WLC.

Repeating the above derivation for unequal driving field amplitudes yields separate conditions for each negative dispersion region. These can be expressed as

$$\chi'(\Delta_C + W + \gamma) - \chi'(\Delta_C + W - \gamma) = -\frac{4\gamma}{\Delta_C + W}. \quad (30)$$

Here, $\Delta_C = \omega_C - W$ denotes the center point of each region or the point at which $\chi'(\omega_C) = 0$ in the case of a negative dispersion slope. For example, for each of the three near-zero absorption and negative dispersion regions in Fig. 3(b), Eq. (30) yields a separate result for the driving fields at each center point to satisfy the WLC. These can then be employed to generate three different resonant bands.

Observe next that when $\omega_{ab} \ll \Omega_\mu^\pm$, the populations $\rho_{aa} \approx \rho_{bb} \approx \rho_{cc}$. Hence, for simplicity, both P_{bc} and P_{ca} can be set to zero in Eqs. (17) and (18) so that only the second term of Eq. (17) and the third term of Eq. (18) remain. The real and imaginary parts of the susceptibility $\chi = \chi' + \chi''$ are then

$$\chi'(\omega) = -\frac{\theta\mathcal{C}\left[-\Delta + \omega_{ab} + \frac{|\Omega_\mu^-|^2}{4\Delta}\right]P_{ad}}{\gamma_{ad}^2 + \left[-\Delta + \omega_{ab} + \frac{|\Omega_\mu^-|^2}{4\Delta}\right]^2} - \frac{\mathcal{C}\left[-\Delta - \omega_{ab} + \frac{|\Omega_\mu^-|^2}{4\alpha^2\Delta}\right]P_{bd}}{\gamma_{bd}^2 + \left[-\Delta - \omega_{ab} + \frac{|\Omega_\mu^-|^2}{4\alpha^2\Delta}\right]^2}, \quad (31)$$

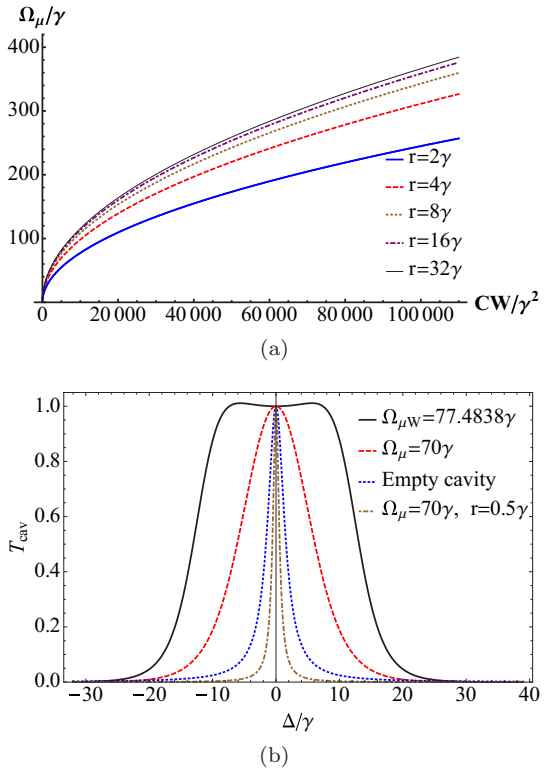

FIG. 4. (a) The driving field $\Omega_{\mu W}$ required to satisfy the WLC condition Eq. (29). (b) The dependence of the cavity transmission on the driving field for $r = 2\gamma$ (except for the inner curve).

$$\chi''(\omega) = -\frac{\theta\mathcal{C}\gamma_{ad}P_{ad}}{\gamma_{ad}^2 + \left[-\Delta + \omega_{ab} + \frac{|\Omega_\mu^-|^2}{4\Delta}\right]^2} - \frac{\mathcal{C}\gamma_{bd}P_{bd}}{\gamma_{bd}^2 + \left[-\Delta - \omega_{ab} + \frac{|\Omega_\mu^-|^2}{4\alpha^2\Delta}\right]^2}, \tag{32}$$

where as usual Δ is $\omega - W$. In driving these equations we assumed that $\gamma_{cd} = 0$ and $\Delta_\mu = 0$. Replotting Figs. 2 and 3 using these expressions leads to almost the same set of curves.

VI. SINGLE WHITE BAND

As noted above, for equal amplitudes of the driving fields $\Omega_\mu^\pm$, e.g., $\alpha = 1$, a single giant resonant frequency band is obtained when the driving field value satisfies a condition corresponding to the WLC of Eq. (29). Figure 4(a), which plots this required field $\Omega_{\mu W}^-$ against $\mathcal{C}$ and r, demonstrates that $\Omega_{\mu W}^-$ is nearly proportional to $\sqrt{\mathcal{C}W}$. For example, for $r = 2\gamma$, a graph of $\Omega_{\mu W}^- = 0.774\,741\sqrt{\mathcal{C}W}$ almost coincides with the plot in Fig. 4(a). As well, $\Omega_{\mu W}^-$ generally increases monotonically with the pumping r; however, the $r = 16\gamma$ and $r = 32\gamma$ curves are nearly identical since the population saturates for large r values.

For $r = 2\gamma$, while previously our calculations employed $\mathcal{C} = \gamma$ as in a standard gas, the previous plot indicates that $\Omega_{\mu W}^- = 774\gamma$. Since this value is unacceptably large, the gas density is decreased by setting $\mathcal{C} = 0.01\gamma$, which yields a more reasonable value of $\Omega_{\mu W}^- = 77.48\gamma$. Hence this scheme for generating a white driving field requires lower pressure compared to previous experiments.

The effect of the white driving field is apparent from the the transmission $T_{\rm cav}$ of the Fabry-Pérot cavity,

$$T_{\rm cav} = \left|\frac{T\, e^{il\omega n(\omega)/c}}{1 - R\, e^{2il\omega n(\omega)/c}}\right|^2, \tag{33}$$

in which T and R are the mirror amplitude transmission and reflection coefficients. The cavity length must equal $l = m\lambda/2 = \pi cm/W$, where m is any integer, to satisfy Eq. (25). The upper exponent is then a function of Δ as $i\pi m(W + \Delta)n(\Delta)/W$, where, in Fig. 4(b), $T = 0.001$, $R = 0.999$, $m = 100$, and $W = 10^6\gamma$. Evidently, in Fig. 4(b) for $\Omega_{\mu W}^-$, the transmission band is broadened significantly compared to that of an empty cavity. The linewidth is additionally nearly 40γ, while additional calculations indicate that the linewidths of the white driving fields are nearly proportional to $\Omega_{\mu W}^{2/3}$. For comparison, the transmission is also plotted for a second value of the driving field, namely, $\Omega_\mu^- = 70\gamma$. The linewidth for this value is less than for the white driving field. We further plot the transmission for $\Omega_\mu^- = 70\gamma$, but with pumping $r = 0.5\gamma$. The pumping clearly reduces the linewidth of the band compared to the empty cavity band since for pumping strengths $r < \gamma$, EIT, which in our scheme leads to a reduced linewidth, is the dominant physical effect in this case.

To summarize, the propagation of light though a cavity with a wide transmission band can be controlled by adjusting the amplitudes of the two driving fields. To activate a white band, the value of Ω_μ^- must be within a certain range that depends on the gas density and the pumping rate according to Fig. 4(a). The linewidth of the transmission band can further be controlled by varying the pumping, gas density, and the white driving field amplitude.

VII. GENERATION OF THREE WHITE BANDS

A. Method A

When the two driving fields are unequal, three negative dispersion regions can be supported, as Figs. 3(b) and 3(d) demonstrate. While the procedure in the previous section can be employed to create a white band in one of the regions, this is not as efficient as white-light generation for $\alpha = 1$. Therefore, we here consider activating all three regions. However, each of these in principle requires a different length. This length must be a half-integer multiple of the center wavelength according to Eq. (25) which, noting that χ' is equal to zero at the center points (Δ_0 and $\Delta_\pm$), yields

$$l\omega_m = cm\pi, \tag{34}$$

for $\mathrm{Re}[n(\omega_C)] = 1$.

Since the cavity length is the product of an integer k, with a half wavelength at frequency $\omega = W$, that is, $l = k\lambda/2 = \pi ck/W$. This yields the condition

$$\omega_m = \frac{mW}{k}. \tag{35}$$

Since the center point of region (0) is found to be $\Delta_0 = 0$, ω_m must equal W, and therefore $m = k$. To ensure that the center points of the regions (± 1) coincide with $\omega_{m\pm1}$,

observe that the center point frequencies $\Delta_\pm$ are $W+\Delta_\pm$ and hence $\omega_{m\pm1} = W+\Delta_\pm$, leading to the conditions $\omega_{m\pm1} = W+\Delta_\pm = \frac{W(m\pm1)}{k} = \frac{W(m\pm1)}{m} = W \pm \frac{W}{m}$ and therefore

$$\Delta_\pm = \pm\frac{W}{m}. \tag{36}$$

Since $W = 10^6$, $\Delta_\pm$ can be approximated by an integer m to satisfy the above equation, however, the condition that $|\Delta_+| = |\Delta_-|$ still remains.

The above results for χ for a given α and Ω_μ^- yield $|\Delta_+| \approx |\Delta_-|$, however, the WLC Eq. (30) requires that the field amplitudes differ in order to generate the regions (±1), implying $|\Delta_+| \neq |\Delta_-|$. For example, employing our current parameter values with $\omega_{ab} = \gamma$ and $\alpha = 3$, we find that the fields required to satisfy the WLCs in Eq. (30) with $\chi'(\omega) = 0$ for the regions (±1) are given by $(\Omega_{\mu W+} = 177.1385\gamma, \Omega_{\mu W-} = 183.7735\gamma)$, where $\Omega_{\mu W\pm}$ are the Ω_μ^- values in the regions (±1). These two values yield $(\Delta_+ = 64.71\gamma, \Delta_- = -67.18\gamma)$. Hence Eq. (36) is not fulfilled and only the regions [(0),(+1)] or [(0),(−1)] will satisfy the WLC.

To circumvent this difficulty we instead set $\omega_{ab} = 0.1\gamma$, and solve the two equations [Eq. (30) with $\chi'(\omega) = 0$]. This gives for region (+1), $\Omega_\mu^- = \Omega_{\mu W+} = 180.1415\gamma$ and $\Delta_+ = 65.8392\gamma$, while for region (−1), $\Omega_\mu^- = \Omega_{\mu W-} = 180.7945\gamma$ and $\Delta_- = -66.0827\gamma$. Here, both $|\Delta_\pm|$ are nearly identical, indicating that for small ω_{ab} the values of $|\Delta_\pm|$ are nearly identical so that Eq. (36) is approximately fulfilled.

Since the two values of $|\Delta_\pm|$ are not precisely identical, we impose Eq. (36) in region (+1) while approximately satisfying this equation in region (−1). This yields, for m in Eq. (36), $k = m = W/\Delta_+ \approx 15188$. The WLC for the region (0) from Eq. (29) then gives $\Omega_{\mu W0} = 169.964\gamma$. Accordingly, the three regions (0),(±1) can be activated in the same cavity.

For simplicity, neglecting the small absorption associated with regions (±1) yields the transmission $T_{\rm cav}$ for the white bands in the three separate wavelength regions with $T_{\rm cav} \approx 1$ illustrated in Fig. 5(a). Of these, the band in region (0) is the widest with a linewidth of $\approx 6\gamma$ Hz, while the linewidth in the (±1) regions is $\approx 3\gamma$ Hz. The three bands are shown individually in Figs. 5(b)–5(d). Evidently, the band of region (−1) in Fig. 5(c) is slightly less broad than that associated with region (+1), since we have employed the driving field corresponding to the latter region. The small depressions in Fig. 5(a) occur in regions of high absorption and therefore can be neglected.

Accordingly, the procedure of this section efficiently produces three different white-light bands in a single cavity. Additionally, the white-light band of region (0) is activated though a driving field of 169.96γ, while to activate the (±1) regions the driving field is found to equal 180.1415γ. This enables the optical switching of the bands.

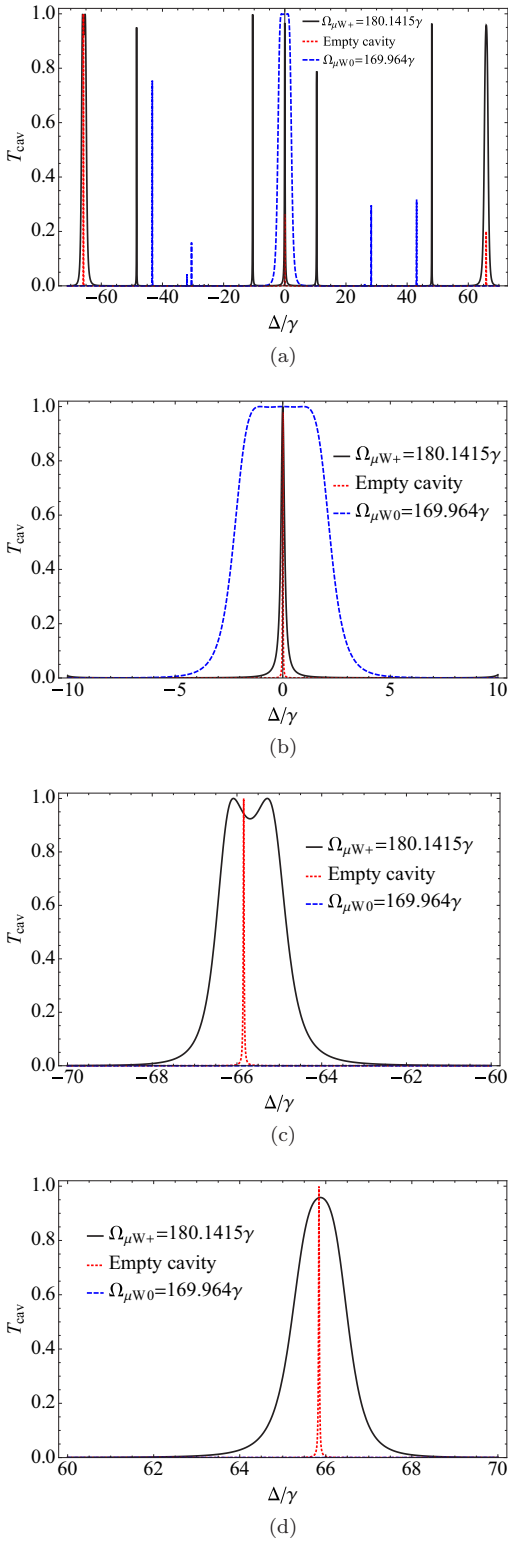

FIG. 5. Cavity transmission frequencies for different driving field values with $\alpha = 3$. (a) All bands together. (b) The band of region (0). (c) The band of region (−1). (d) The band of region (+1).

B. Method B

In Sec. VII A, three white bands were generated subject to the condition $\omega_{ab} \approx 0$. This and the following section instead outline two procedures for generating three bands in which the value of ω_{ab} is not constrained. The first of these procedures assumes that the length of the cavity can be altered. In this case, the cavity condition, Eq. (25), for region (0) reads

$$l_0 W = cm\pi, \quad l_0 = \frac{m\pi c}{W}, \tag{37}$$

while the condition for the other two regions (± 1) with varying length can be written as

$$l_{\pm}(W+\Delta_{\pm}) = cm\pi, \quad l_{\pm} = \frac{cm\pi}{W+\Delta_{\pm}}\frac{W}{W}, \tag{38}$$

and therefore

$$l_{\pm} = l_0\left(\frac{1}{1+\frac{\Delta_{\pm}}{W}}\right) = l_0 X_{\pm}, \tag{39}$$

where $X_{\pm}$ are multiplicative factors that express the required length modifications. Setting ω_{ab} to its previous value, γ, and calculating the driving fields that satisfy the white cavity condition for $\alpha = 3$ yields ($\Omega_{\mu W0} = 169.94\gamma$, $\Omega_{\mu W+} = 177.13\gamma$, $\Omega_{\mu W-} = 183.77\gamma$) for the [(0), (+1), (−1)] regions, respectively. If the length of region (0) is set to $l_0 = 100\pi c/W$, the required lengths of the (± 1) regions are $l_+ = 0.999\,935\,28 l_0$ and $l_- = 1.000\,067\,19 l_0$, which are sufficiently close to l_0 to enable the tuning of the cavity length.

The cavity transmission is plotted in Fig. 6, demonstrating three bands with a very large linewidth (≈1.0 GHz) compared to that of the previous method since the cavity length is reduced. Recall as well that for $\alpha = 1$, the band of region (0) is nearly unchanged but requires a smaller amplitude driving field, as evident from Fig. 4(b). Further, as in the previous section, the center frequency of the (± 1) bands can be shifted by adjusting the $\mathcal{C}$ parameter. Hence here again both the linewidth and the center of the transmitted bands can be easily manipulated.

C. Method C

A third procedure for generating three white bands which employs $\alpha = 1$ is to tune the spacing energy ω_{ab}. We notice in Fig. 3 that there are two peaks on either side of the transmission maximum. These peaks are related to ω_{ab} as they vanish for $\omega_{ab} = 0$. Increasing ω_{ab} therefore results in three white bands similar to the $\alpha \neq 1$ case. The width of both regions (± 1) approximately equals ω_{ab}, while the bandwidth of the middle region (0) is $\Omega_{\mu}^{-} \approx \omega_{ab}$. Therefore, when $\Omega_{\mu}^{-} \approx 2\omega_{ab}$, the three regions will possess almost the same width. This method could be highly efficient if ω_{ab} is easily tunable and illustrates that three bands can be generated even for equal amplitude driving fields.

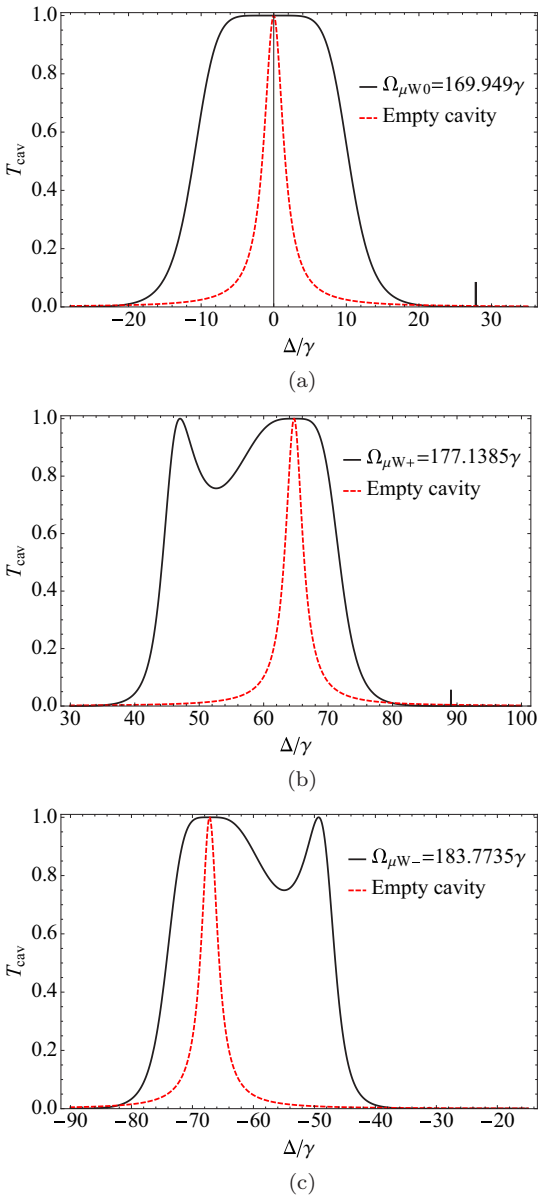

FIG. 6. Magnified plots of the transmission bands of the cavity for differing driving field amplitudes with $\alpha = 3$ for cavity lengths (a) l_0, (b) $l_+ = l_0 X_+$, and (c) $l_- = l_0 X_-$.

VIII. ONE WHITE BAND WITH ADJUSTABLE CENTER FREQUENCY

Finally, we propose a technique for generating a single large white band with a center frequency that can be displaced by adjusting the parameter α. We specialize here to method B, for which $\omega_{ab} = \gamma$. Solving for the white cavity condition Eq. (30), along with $\chi' = 0$, yields the value of the field that satisfies the WLC condition $\Omega_{\mu W\pm}$ as well as the center point $\Delta_{\pm}$ for each value of α. These results are shown in Fig. 7, where Fig. 7(a) plots $\Omega_{\mu W\pm}$ against the ratio $1/\alpha$ while Fig. 7(b) displays the dependence of the center point location on of the same ratio. Figure 7(a) demonstrates that there is almost a constant spacing between $\Omega_{\mu W-}$ and $\Omega_{\mu W+}$, which is expected since ω_{ab} is not negligible, as discussed in Sec. VII A. Further, both $\Omega_{\mu W\pm}$ increase rapidly as α approaches 1 as the widths of the (± 1) regions decrease in this limit and vanish when $\alpha = 1$. The position of the center points in Fig. 7(b) behaves similarly.

The above figures can be employed as follows. To position the white-light band around a given center point, e.g., $\Delta_{\pm} = x$, the value of α can be determined from Fig. 7(b) and the required driving fields Ω_{μ}^{-} and $\Omega_{\mu}^{+} = \Omega_{\mu}^{-}/\alpha$ are then obtained from Fig. 7(a). Finally, the cavity length must be adjusted to equal $l = X_{\pm} l_0$. A similar procedure for displacing the white band position can be formulated for method A, however, the resulting curves differ since ω_{ab} is altered in this scenario. The only positions which cannot be accessed fall in the interval $\approx -37.2\gamma$ to 35.5γ, as evident from Fig. 7(b). The two edges of this range correspond to $\alpha \to \infty$, which limits the two regions present in Fig. 3(d).

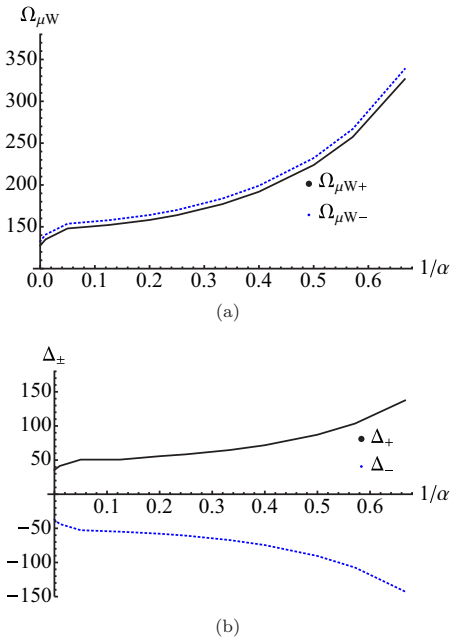

FIG. 7. The (a) driving fields $\Omega_{\mu}^{-} = \Omega_{\mu W\pm}$ and (b) center point positions $\Delta_{\pm}$ resulting from the white-light condition for the (± 1) regions plotted as a function of the ratio $1/\alpha$.

IX. POTENTIAL APPLICATIONS

While the practical implementation of the systems described above cannot be specified exactly without considerable additional experimental and presumably theoretical analyses, a comparison with theoretical as well as the limited experimental results of similar studies suggest several obvious applications. One of these is all-optical switches for which, for example, the performance of an optically switched nonlinear ring cavity [41,42] can be significantly enhanced by introducing doped Λ atoms into the ring cavity. The Λ scheme then exhibits a negative dispersion slope, enabling the resonator to operate in a tunable white-light band [17] region with reduced switching time and power.

Such systems could possibly extend existing single-band optical switching applications of white-light bands [1–6,43] by enabling light to be optically or mechanically switched or modulated within two or three wavelength bands simultaneously within an optical cavity. Introducing double-Λ atoms into the resonator of a single-band switch not only generates multiple white bands that can be simultaneously modulated, but also removes the limitation of a standard undoped resonator which is not easily adjusted after fabrication.

Measurement applications such as gravitational-wave detection are often based on scanning a wide frequency band [41,44] in order to determine the wavelength dependence of relevant physical properties. While white-light cavities are employed to accumulate data over wide continuous ranges of frequencies rather than a limited set of discrete frequencies, employing a double-Λ system would extend this capability by enabling the center frequency to be adjusted without significantly affecting the measurement bandwidth. Finally, multiband systems could be applied to numerous additional fields as, for example, quantum optics and information.

X. CONCLUSION

This article has demonstrated that one, two, or three white bands can be generated in a single cavity simply by adjusting the magnitude of the driving fields and the cavity length. Three separate techniques with different relative advantages were given for creating three white bands. As well, the wavelengths of the white-light bands can be further shifted through optical or mechanical tuning. As a consequence, the three-band system can be more efficiently controlled compared to previously proposed single white-light band systems.

In the future, this work could possibly be extended to the production of three simultaneous white bands with only a single driving field. Further, for systems with a greater number of interactions between the probe beam and the atom than those considered above, the number of white cavity bands could in principle be further increased [45,46].

ACKNOWLEDGMENTS

A.O. acknowledges financial support from Taibah University and gratefully acknowledges the hospitality at KACST where this work was done. This work is further supported by grants from the King Abdulaziz City for Science and Technology (KACST) and the National Science and Engineering Council of Canada.

[1] R. X. Adikhari, Rev. Mod. Phys. **86**, 121 (2014).
[2] A. Buonanno and Y. Chen, Phys. Rev. D **67**, 062002 (2003).
[3] T. Shigeki, M. Masanao, and S. Seiji, Opt. Lett. **36**, 2812 (2011).
[4] M. Skorczakowski, J. Swiderski, W. Pichola, P. Nyga, A. Zajac, M. Maciejewska, L. Galecki, J. Kasprzak, S. Gross, A. Heinrich, and T. Bragagna, Laser Phys. Lett. **7**, 498 (2010).
[5] P. Peng and F.-L. Li, Phys. Rev. A **75**, 062320 (2007).
[6] J. I. Cirac, P. Zoller, H. J. Kimble, and H. Mabuchi, Phys. Rev. Lett. **78**, 3221 (1997).
[7] H. J. Kimble, Nature (London) **453**, 1023 (2008).
[8] L.-M. Duan and C. Monroe, Rev. Mod. Phys. **82**, 1209 (2010).
[9] L.-G. Wang, M. Ikram, and M. S. Zubairy, Phys. Rev. A **77**, 023811 (2008).
[10] J.-X. Zhang, H.-T. Zhou, D.-W. Wang, and S.-Y. Zhu, Phys. Rev. A **83**, 053841 (2011).
[11] H.-T. Zhou, D.-W. Wang, D. Wang, J.-X. Zhang, and S.-Y. Zhu, Phys. Rev. A **84**, 053835 (2011).
[12] D. Yafan, L. Gongwei, Z. Shicheng, N. Yueping, and G. Shangqing, Opt. Commun. **358**, 73 (2016).
[13] B. Dayan, A. S. Parkins, T. Aoki, E. P. Ostby, K. J. Vahala, and H. J. Kimble, Science **319**, 1062 (2008).
[14] A. W. Brown and M. Xiao, Opt. Lett. **30**, 699 (2005).
[15] X. M. Su and B. S. Ham, Phys. Rev. A **71**, 013821 (2005).

[16] R. Sadighi-Bonabi, T. Naseri, and M. Navadeh-Toupchi, Appl. Opt. **54**, 368 (2015).
[17] J. Xu, M. Al-Amri, Y. Yang, S.-Y. Zhu, and M. S. Zubairy, Phys. Rev. A **86**, 033828 (2012).
[18] G. S. Pati, M. Salit, K. Salit, and M. S. Shahriar, Phys. Rev. Lett. **99**, 133601 (2007).
[19] R. H. Rinkleff and A. Wicht, Phys. Scr. **T118**, 85 (2005).
[20] A. Rocco, A. Wicht, R.-H. Rinkleff, and K. Danzmann, Phys. Rev. A **66**, 053804 (2002).
[21] A. Wicht, K. Danzmann, M. Fleischhauer, M. Scully, G. Miller, and R. H. Rinkleff, Opt. Commun. **134**, 431 (1997).
[22] Q. Sun, M. S. Shahriar, and M. S. Zubairy, Phys. Rev. A **81**, 033826 (2010).
[23] H. N. Yum, X. Liu, Y. Jang, M. Kim, and M. S. Shahriar, IEEE J. Lightwave Technol. **29**, 2698 (2011).
[24] H. N. Yum, J. Scheuer, M. Salit, P. R. Hemmer, and M. S. Shahriar, IEEE J. Lightwave Technol. **31**, 3865 (2013).
[25] H. N. Yum, M. E. Kim, Y. J. Jang, and M. S. Shahriar, Opt. Express **19**, 6705 (2011).
[26] M. Salit and M. S. Shahriar, J. Opt. **12**, 104014 (2010).
[27] H. N. Yum, M. Salit, J. Yablon, K. Salit, Y. Wang, and M. S. Shahriar, Opt. Express **18**, 17658 (2010).
[28] O. Kotlicki, J. Scheuer, and M. S. Shahriar, Opt. Express **20**, 28234 (2012).
[29] K.-J. Boller, A. Imamoglu, and S. E. Harris, Phys. Rev. Lett. **66**, 2593 (1991).
[30] M. Mücke, E. Figueroa, J. Bochmann *et al.*, Nature (London) **465**, 755 (2010).
[31] P. P. Orth, R. Hennig, C. H. Keitel, and J. Evers, New J. Phys. **15**, 013027 (2013).
[32] A. A. Othman and D. Yevick, J. Mod. Opt. **64**, 1208 (2017).
[33] M. O. Scully, Phys. Rev. Lett. **67**, 1855 (1991).
[34] Y. Zhang, Y.-M. Liu *et al.*, Opt. Commun. **343**, 183 (2015).
[35] Y.-W. Lin, W.-T. Liao, T. Peters, H.-C. Chou, J.-S. Wang, H.-W. Cho, P.-C. Kuan, and I. A. Yu, Phys. Rev. Lett. **102**, 213601 (2009).
[36] M. Cheneau *et al.*, Europhys. Lett. **83**, 60001 (2008).
[37] D. F. Phillips, A. Fleischhauer, A. Mair, R. L. Walsworth, and M. D. Lukin, Phys. Rev. Lett. **86**, 783 (2001).
[38] C. Liu, Z. Dutton, C. H. Berhoozi, and L. V. Hau, Nature (London) **409**, 490 (2001).
[39] E. A. Korsunsky and D. V. Kosachiov, Phys. Rev. A **60**, 4996 (1999).
[40] D. Arsenović and J. Dimitrijević, Phys. Scr. **T149**, 014008 (2012).
[41] J. E. Heebner and R. W. Boyd, Opt. Lett. **24**, 847 (1999).
[42] C. Li, N. Dou, and P. Yupapin, J. Opt. A: Pure Appl. Opt. **8**, 728 (2006).
[43] W. K. Chang, Y. H. Chen, and J. W. Chang, Opt. Lett. **35**, 2687 (2010).
[44] B. P. Abbott *et al.* (LIGO Scientific Collaboration and Virgo Collaboration), Phys. Rev. Lett. **116**, 061102 (2016).
[45] T. Biwa, Y. Ueda, H. Nomura, U. Mizutani, and T. Yazaki, Phys. Rev. E **72**, 026601 (2005).
[46] N. Li, J. Xu, G. Song *et al.*, Phys. Rev. A **93**, 043819 (2016).